Identifying spectral features of characteristics of *Sphagnum* to assess the remote sensing potential of peatlands: A case study in China

Y. Pang[1,2], Y. Huang[1,2], Y. Zhou[1,2], J. Xu[1,2], Y. Wu[3]

[1] Institute of Remote Sensing and Geoscience, Hangzhou Normal University, Zhejiang, China
[2] Key Laboratory of Urban Wetland and Regional Change in Zhejiang Province, Zhejiang, China
[3] College of Life and Environmental Sciences, Hangzhou Normal University, Zhejiang, China

SUMMARY

Sphagnum mosses are the dominant species of natural peatlands, which are important in the global carbon cycle. There is increasing interest in the use of sensors mounted on satellites or unmanned aerial vehicles in association with management of the ecological resources of peatlands, e.g. for monitoring purposes. Since *Sphagnum* mosses grow with many other vascular plants in the same habitat, the spectral signals of *Sphagnum* moss pixels in the remote sensing image are mixed, so investigation of their spectral characteristics forms a basis for remote sensing of peatlands. In this study, the spectral characteristics of *Sphagnum magellanicum* Brid were analysed at various levels (field and laboratory hyperspectral, laboratory plant physiology, satellite sensors) and compared with those of other plants, in order to examine the potential for developing remote sensing methods to distinguish *Sphagnum*. The results showed that: (1) the unique spectral characteristics of *S. magellanicum* that might be used to distinguish it from other plants are located in the near-infrared and shortwave infrared (NIR-SWIR; 760–2400 nm) region of the reflectance spectrum, and especially in the two water absorption bands (980 and 1150 nm); (2) the cell structure of *S. magellanicum* (which is the basis of its large water-holding capacity) explains the very low reflectance in the NIR-SWIR and the sensitivity of reflectance in the IR to moisture; and (3) the identification of *Sphagnum* from satellite remote sensing data should be based on sensors which have more infrared channels such as Sentinel-2A MSI, and on vegetation indices established in the NIR-SWIR such as MSI (moisture stress index) and NDII (normalised difference infrared index).

KEY WORDS: hydrological stress, plant ecology, *Sphagnum magellanicum*, vegetation indices

INTRODUCTION

Peatlands are wetland ecosystems that accumulate peat. They cover only 2–3 % of the global land area (Dahl & Zoltai 1997) but are estimated to store 500 ± 100 Pg of carbon (Yu 2012), which is one-third of the global soil carbon pool (Gorham 1991, Limpens *et al.* 2008). More than 50 % of peatland carbon has been fixed by mosses belonging to the genus *Sphagnum* (Vogelmann & Moss 1993). *Sphagnum* is a cosmopolitan genus found on all continents except Antarctica (Kyrkjeeide *et al.* 2016) and is considered to be an indicator of global climate change (Whinam & Copson 2006) because it has a strong carbon sequestration capacity that is environmentally sensitive (Dise 2009, Wu 2012). For example, elevated temperatures and increased concentrations of carbon dioxide in the atmosphere will reduce its accumulated biomass (Schultheis *et al.* 2010). Especially now that the importance of peatlands in global carbon cycling is widely recognised, the availability of remote sensing techniques capable of distinguishing *Sphagnum* from other plants will become increasingly important to help scientific researchers and land managers better understand the spatial distribution and disposition of relatively natural peatlands.

Sphagnum magellanicum Brid is one of the most widely distributed species in the world (Kyrkjeeide *et al.* 2016) and is frequently used as a model to understand *Sphagnum* physiology (Hanson & Rice 2014) and ecology (Vitt & Weider 2008). Thus, an

ability to determine its distribution at regional and global scales could be an important tool in assessing large-scale trends in the ecological functioning and degradation of peatlands. In this context, remote sensing can provide consistent and continuous spatial coverage of large areas, unlike traditional plant surveys which require ground-based inspections and are, therefore, time-consuming and costly.

When using remote sensing for *Sphagnum* mapping, it is necessary to distinguish the characteristic spectral features of *Sphagnum* from those of other plants, and an extensive spectral analysis of plants can be helpful in this regard (Xie *et al.* 2008, Domínguez-Beisiegel *et al.* 2016). Currently, broadleaf (Plate model - PROSPECT) (Jacquemoud & Baret 1990) and coniferous (LIBERTY) (Dawson *et al.* 1998) radiation transmission models have been established, but there is still a large knowledge gap for bryophytes.

Vogelmann & Moss (1993) compared the reflectance spectra of different *Sphagnum* species, showing that there are large differences in the visible (VIS, 380–760 nm) and near-infrared regions (NIR, 1000–2400 nm). Bubier *et al.* (1997) compared *Sphagnum* with several vascular plants by hyperspectral analysis and found that mosses exhibit distinctly different spectral characteristics from vascular plants in the visible, near-infrared (NIR) and shortwave infrared (SWIR) regions. However, these two studies did not link plant physiology to the spectrum.

Bryant & Baird (2003) tested the spectra (400–2,500 nm) of *Sphagnum* under different hydrological conditions to describe the moisture monitoring capability of remote sensing for peatlands. Because *Sphagnum* is sensitive to changes in water level (Rydin & Jeglum 2006), subsequent studies have focused on the extraction and application of hydrological features (Harris *et al.* 2005, 2006) and established a remote sensing hydrological monitoring model for peatlands (Letendre *et al.* 2008, Harris & Bryant 2009). However, the response of *Sphagnum* spectra to short-term water shortage has rarely been considered.

While previous remote sensing studies have described the spectral characteristics of *Sphagnum* and applied hydrological inversion (Bryant & Baird 2003, Harris *et al.* 2005, 2006; Letendre *et al.* 2008, Harris & Bryant 2009), there are still some limitations. First, *Sphagnum* is usually mixed in with vascular plants (Rydin & Jeglum 2006) whose spectral characteristics often dominate the pixel spectra of medium-sized to large images. This not only affects the purity of the *Sphagnum* signal (Sonnentag *et al.* 2007) but also causes errors in biological interpretation, such as leaf pigment content (Cole *et al.* 2014). Therefore, further studies are required to clarify the spectral characteristics of *Sphagnum* within specific bands and to explain the physiological mechanisms of these bands, in preference to roughly obtaining these characteristics from the spectrum (Vogelmann & Moss 1993, Bubier *et al.* 1997). Secondly, few studies have systematically assessed the potential of earth observation (EO) satellites for the identification of peatland species (Buermann *et al.* 2008, Wu & Peng 2011, Cord *et al.* 2013). In particular, the latest EO sensor (Sentinel-2A MSI) has been proven to detect vegetation changes with high accuracy (Radoux *et al.* 2016). Moreover, existing remote sensing monitoring systems for peatlands often use established vegetation indices such as the NDVI and/or the EVI (Douma *et al.* 2007, Schubert *et al.* 2010) which, although they have been proven to work well in ecological monitoring, cannot necessarily be used directly to detect *Sphagnum* (or any other moss). Remote sensing of vegetation relies on the reflectance properties of the target object, which is controlled by three factors: leaf pigment (400–760 nm), cell structure (760–1300 nm) and water content (1300–2500 nm). *Sphagnum* contains the unique red pigment sphagnorubin (detected at 400–760 nm), which is found on its cell walls (Tutschek 1982, Gerdol 1996). Also, it has no palisade layer or spongy tissue and is structurally distinct from vascular plants in that its leaves are monolayered with only two cell types (Goetz & Price 2015), comprising a network of large, transparent hyaline cells and normal photosynthetic cells with chlorophyll (Kremer *et al.* 2004) (detected at 760–1300 nm). Moreover, it has a strong water-holding capacity and can soak up water like a sponge (detected at 1,300–2,500 nm). After water absorption, *Sphagnum* can attain a weight 20 times its dry weight.

Because sensors vary in their ability to distinguish *Sphagnum* from other species that grow in the same plant communities, studies are needed to explain the

underlying causes of the differences in spectral reflectance characteristics, as well as to explore the potential for using existing satellite sensors and vegetation indices to detect these differences (Pu *et al*. 2005, Xie *et al*. 2008). In this study (flow diagram in Figure 1), the following questions are addressed:

(1) What are the special and stable spectral ranges for *Sphagnum*?

(2) Which multispectral satellites and which vegetation indices are most suitable for mapping *Sphagnum*?

We compare the spectra of *Sphagnum*, *Phyllostachys heteroclada* Oliver which grows in close association with *Sphagnum* on our site, and other plants selected to represent the general groups of coniferous and broad-leaved species, as well as lichens. The effects of physiological (water) stress on the spectral regions associated with *Sphagnum* have also been analysed. Additionally, we compare the performance of four multi-spectral satellite sensors and four vegetation indices in distinguishing *Sphagnum* from other plants.

METHODS

Study site

Tianbaoyan National Nature Reserve (TNNR; 117° 28' 3" to 117° 35' 28" E, 25° 50' 51" to 26° 1' 20" N; Figure 2) is located in Fujian Province, China. The climate of the region is mid-subtropical oceanic monsoon, with a mean annual temperature of 15 °C, annual precipitation of 2,039 mm which falls mostly between May and September, and an annual relative humidity >80 % (Xiao *et al*. 2018).

The 30.7 ha peatland selected for this study is located within the Nature Reserve, at Tiandou Mountain. The peat layer is 10–25 cm thick and relatively wet, with a natural soil moisture content of 33 %. The surface of the peatland has hummock-hollow microtopography with surface runoff, and there is a beaver pond at the mire margin (Figure 3a). The peatland's vegetation can be divided into categories based on the four dominant species, namely: *S. magellanicum*, *P. heteroclada*, *Palhinhaea cernua* (Linn.) Vasc. et Franco and *Juncus effusus* Linn. Total coverage within the site's plant communities can reach 100 %. More information on the vegetation of *Sphagnum* peatlands in the TNNR can be found in Huang (2009).

The mixed *P. heteroclada* and *S. magellanicum* community was selected for field collection of spectral data because this community is a special vegetation type for mid-latitude *Sphagnum* peatlands, with a shrub layer of height 50–300 cm dominated by *P. heteroclada* and a ground layer dominated by *S. magellanicum* (Figure 3b). In this community, *S. magellanicum* varies in colour depending on the growth conditions; in general, *S. magellanicum* will be red in open areas and green when shaded.

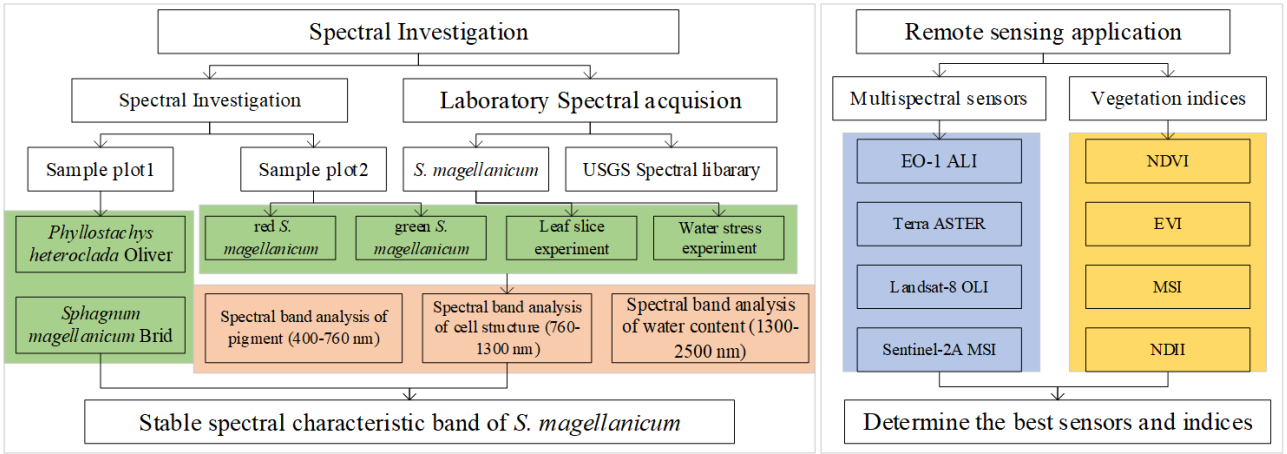

Figure 1. The research flow diagram, which consists of two parts. On the left is spectral analysis, where green rectangles represent spectral acquisition and the pink rectangle represents plant physiology-spectral analysis. On the right is remote sensing simulation, where the blue rectangle encompasses four multispectral sensors and the orange rectangle four vegetation indices.

Acquisition of spectra in field and laboratory

To measure the spectral reflectance of peatland vegetation, an ASD FieldSpec3 spectroradiometer with a nominal spectral range of 350–2500 nm was used.

In the field, two plots were identified within different vegetation communities. Plot 1 was located in *P. heteroclada* and *S. magellanicum* mixed habitat (Figure 4a) and Plot 2 was in open *S. magellanicum* habitat (Figure 4b). Acquisition of the field spectra involved measurement of a calibrated reference panel (a white disc of diameter 0.2 m) followed by vegetation scenes of similar size, under consistent cloud-free conditions. All measurements were repeated three times with an average of ten scans per measurement (total of 30 scans per scene). Target reflectance was calculated from the ASD measurements using a panel substitution methodology.

In Plot 1 we collected the spectra of a single scene of *P. heteroclada* (Figure 5a), two scenes of red *S. magellanicum* and two scenes of green

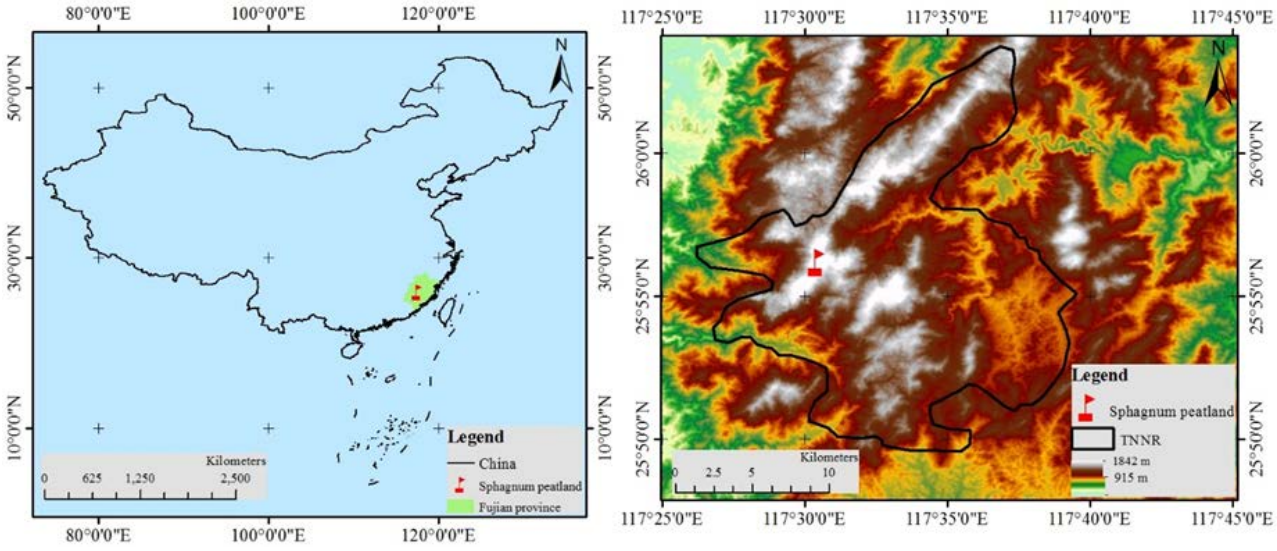

Figure2. Maps showing the location of the study site in Fujian Province, China (left); and within the Tianbaoyan National Nature Reserve (TNNR), superposed on ASTER GDEM base map (right).

(a) (b)

Figure 3. (a) View of the study site, which is a *Sphagnum* bog in TNNR. (b) *P. heteroclada* and *S. magellanicum* plant community on the study site (from Pang *et al*. 2019).

S. magellanicum (Figure 5b). In Plot 2 we collected the spectra of three different scenes of *S. magellanicum*, referred to as 2.1, 2.2 and 2.3, respectively (Figure 5c). We then calculated average spectra for each scene (based on 30 scans per scene) and some combined scenes (e.g. for both green and red *S. magellanicum* in Plot 1, 60 scans each).

In the laboratory, a darkroom was constructed with a 1,000 W halogen lamp as the light source. *S. magellanicum* spectra (three repetitions, each averaging ten scans whilst rotating the sample through 120°) were collected using a 25° bare fibre field of view (FOV) at distance 0.15 m from the sample (Figure 5d).

Spectral comparison between different peatland plant species will help to determine the characteristic spectral bands of *Sphagnum*. However, archived field spectra for peatland plants were not available, so we selected spectra for the closest substitute species from the USGS spectral library (https:// minerals. usgs.gov/science/spectral-library) (Kokaly *et al.* 2017). Peatlands in northern latitudes are predominantly forested, and are normally dominated by spruce trees, shrubs, *Sphagnum* and lichens (Richardson *et al.* 2018). Therefore, the library spectra chosen were: (1) *Quercus robur L* (common oak), which belongs to the beech and oak family Fagaceae; (2) *Picea engelmannii* Parry ex Engelm (Engelmann spruce), as an example species from the Pinaceae; (3) *Spartina alterniflora* Loisel, a wetland grass from the Poaceae; and (4) a lichen identified as '*Licedea* sp.' (probably meaning *Lecidea*).

Figure 4. (a) Field spectroscopy (ASD FieldSpec3) setup for spectral characterisation of the vegetation at Plot 1 (*P. heteroclada* and *S. magellanicum* community); (b) *S. magellanicum* at Plot 2.

Figure 5. Samples of plant species and the laboratory darkroom. (a) *P. heteroclada* in Plot 1; (b) red and green *S. magellanicum* in Plot 1; (c) green *S. magellanicum* in Plot 2; (d) the indoor spectroscopy (ASD FieldSpec3) setup used for the water content gradient experiment. (a) and (c) from Pang *et al*. (2019).

Acquisition and processing of satellite sensor spectra

Spectra were obtained from four satellite sensors, namely: Earth Observing-1 Advanced Land Imager (EO-1 ALI), Terra Advanced Spaceborne Thermal Emission and Reflection Radiometer (ASTER), Landsat-8 Operational Land Imager (OLI) and Sentinel-2A MultiSpectral Instrument (MSI). Data from these sensors have been used widely in vegetation monitoring, and thus have possible potential for *Sphagnum* identification or mapping. In this study, we used filter functions of the four multispectral sensors to convert the field or laboratory spectra for our focus plants to satellite spectra. Using the appropriate formulae (Table 1), we also calculated four vegetation indices, namely: normalised difference vegetation index (NDVI), enhanced vegetation index (EVI), moisture stress index (MSI), and normalised difference infrared index (NDII).

Spectral processing

The field spectra were distorted by atmospheric moisture. Therefore, we applied the intensity test method proposed by Wang *et al*. (2009) to eliminate the abnormal spectra and retain the effective bands: 400–1350 nm, 1450–1750 nm and 2000–2400 nm. The spectra collected in the laboratory were less affected by ambient light and atmospheric noise than those collected in the field, so for these we retained the whole 400–2500 nm band. Spectral processing methods can be used to amplify and accurately obtain the spectral characteristics of a target. Here, the first-order and second-order derivative reflectance spectra (FDR and SDR) and the logarithm of reciprocal spectra [lg(1/R)] (Liu *et al*. 2016) were calculated.

Table 1. Sensor-specific broad-band spectral indices employed in this study.

Index	Platform	Equation	Reference	Usage
NDVI	EO-1 Terra Sentinel-2A Landsat-8	$(R_{nir} - R_{red}) / (R_{nir} + R_{red})$	Deering (1979)	commonly used to monitor vegetation growth status, coverage, etc.
EVI	ALI Sentinel-2A Landsat-8	$2.5*(R_{nir} - R_{red}) / (R_{nir}+6.0*R_{red}7.5* R_{blue}+1)$	Wardlow *et al.* (2007)	
EVI_2	Terra	$2.5*(R_{nir} - R_{red}) / (R_{nir}+2.4*R_{red}+1)$	Jiang *et al.* (2008)	
MSI	EO-1 Terra Sentinel-2A Landsat-8	R_{swir} / R_{nir}	Hunt & Rock (1989)	generally used to invert or monitor the moisture content of plant leaves
NDII	EO-1 Terra Sentinel-2A Landsat-8	$(R_{nir} - R_{swir}) / (R_{nir} + R_{swir})$	Hardisky *et al*. (1983)	

The derivative spectra can greatly reduce the soil background, and the logarithmic method can reliably reflect the differences between similar spectra (Plaza *et al.* 2009). Due to the spectral intervals, the derivative spectra are usually estimated using a differential method. The formulae are, for FDR:

$$\mathrm{R}'(\lambda_i) = \frac{R(\lambda_{i+1}) - R(\lambda_i)}{\lambda_{i+1} - \lambda_i} \quad [1]$$

for SDR:

$$\mathrm{R}''(\lambda_i) = \frac{R\prime(\lambda_{i+1}) - R\prime(\lambda_i)}{\lambda_{i+1} - \lambda_i} \quad [2]$$

and for lg(1/R):

$$\lg(1/\mathrm{R}) = lg(1/\mathrm{R}(\lambda_i)) \quad [3]$$

where λ_i represents the wavelength value at band i, $R(\lambda_i)$ is the reflectance at λ_i, $R'(\lambda_i)$ and $\mathrm{R}''(\lambda_i)$ are the first-order and second-order derivatives, respectively, and lg(1/$R(\lambda_i)$) is the logarithm of the $R(\lambda_i)$ reciprocal.

***Sphagnum*: structure and physiology**

We explored the effects on *S. magellanicum* spectra of (i) leaf pigment (spectral range 400–760 nm), (ii) cell structure (760–1300 nm) and (iii) water content (1300–2500 nm).

Effects of leaf pigment

The spectra of red and green *S. magellanicum* acquired from Plot 1 were compared to illustrate the effect of the difference in their pigment complements on the reflectance of visible light (VIS; 400–760 nm).

Effects of cell structure

Cell structure comparisons have been used to identify moss genera and *Sphagnum* species (Mendes & Dias 2013). The unique cellular structure of *Sphagnum* means that controlled NIR spectra are the optimal bands for *Sphagnum* identification. Sections of fresh and dried leaves and stems of the *S. magellanicum* from our study site were observed in order to reveal the contribution of its cellular structure to its near infra-red (NIR; 760–1300 nm) spectral characteristics. The sizes and shapes of cells in the leaves and in the cross-section of the stem were observed in fresh *S. magellanicum* using a stereo microscope (Leica EZ4 HD), and photographed under an Olympus optical microscope. Additionally, the structure of dried leaves was examined by observing them under an Axiovert 40 CFL inverted fluorescence microscope.

Effects of water content

A water content gradient experiment was conducted to determine the correlation between leaf moisture content and the short-wave infra-red (SWIR; 1300–2500 nm) reflectance of the *S. magellanicum* This experiment involved a short-term (5-day cycle) dehydration process simulation on *S. magellanicum* in the laboratory (Harris 2008, Van Gaalen *et al.* 2007). Samples of *S. magellanicum* (collected from Plot 2) were held at 25 °C and 40 % relative humidity for 24, 48, 72, 96 and 120 hours, respectively, to simulate different degrees of water loss. The fresh state, meaning no water shortage or sufficient water, corresponded to 0 hours and the state of complete dehydration by the dryer was reached after 144 hours. At each time point, the reflectance spectrum was recorded in the laboratory darkroom using the ASD spectroradiometer (Figure 5d).

RESULTS

Spectral characteristics of *Sphagnum* and other plant species

In general, the spectra of vascular plants (represented by *Quercus robur*, *Picea engelmannii* and *Spartina alterniflora*), mosses (*S. magellanicum*) and lichens (‘*Licedea* sp.’) vary widely (Figure 6). In the VIS (400–760 nm), all plants except the lichen have similar spectral patterns with a peak at ~550 nm (shown as P1 in Figure 6) representing the electromagnetic radiation absorption band associated with leaf pigment. *S. magellanicum* has the lowest reflectance, and its peak corresponds to the shortest wavelength. The IR spectra are more distinguishable. In the NIR (760–1350 nm), other plants (apart from the lichen) have a higher reflection platform than *S. magellanicum*, and two reflectance troughs (shown as T1 and T2 in Figure 6) at longer wavelengths than for *S. magellanicum*. Plant reflectance in the SWIR (1350–2500 nm) is quite low, especially for

S. magellanicum, corresponding to its higher water-holding capacity. The spectrum for the lichen (‘*Licedea* sp.’) is distinctive across the entire spectral range (320–2450 nm), meaning that it can easily be separated from other vegetation. Moreover, the spectral properties of *S. magellanicum* in the VIS, NIR and SWIR are distinguishable from those of other plants, forming a basis for extraction of this species by remote sensing.

Differences in spectral reflectance between *P. heteroclada* and *S. magellanicum*

The distinctive characteristics of *S. magellanicum*’s reflectance of different colours are concentrated in the VIS range (400–760 nm) (Figure 7). Green *S. magellanicum* and *P. heteroclada* have similar reflectance peaks at approximately 560 nm (P1 in Figure 7), while red *S. magellanicum* has a peak nearer to red light, at approximately 620 nm. In the VIS-NIR range (400–1000 nm), red *S. magellanicum* has much lower reflectivity than green *S. magellanicum*. All samples have troughs at 680 nm, as well as in the NIR near 980 nm and 1150 nm. Furthermore, the reflectance values of the five *S. magellanicum* samples are quite low, with a high degree of similarity in the SWIR (1450–2400 nm), except for *S. magellanicum* 2.3.

In the *P. heteroclada* and *S. magellanicum* community, the spectral region for *S. magellanicum* extraction is located in the range 900–1200 nm (NIR), and especially at 980 nm and 1150 nm. Throughout the spectral range (400–2400 nm), reflectance is always lower for *S. magellanicum* than for *P. heteroclada*, especially in the SWIR (1450–2400 nm) (Figure 8a). After logarithmic transformation (Figure 8b), the distinctions between 560 nm and 675 nm and between 980 nm and 1150 nm can be seen clearly. In Figure 8c, the peaks of *P. heteroclada* and green *S. magellanicum* are almost coincident at approximately 520 nm, then the derivative values decrease and reach a minimum at 574 nm (-0.04 %, shown as P1 in Figure 8c). In the 500–600 nm range, the *S. magellanicum* FDR decreases steadily until it reaches 0 at 633 nm, and there is no prominent peak in this interval (P2 in Figure 8c). The highest peak for all three of the samples shown is at 700 nm (P3 in Figure 8c), and there are gaps between the peaks for these samples. The gap in FDR value between *P. heteroclada* and *S. magellanicum* is largest in the NIR, especially at

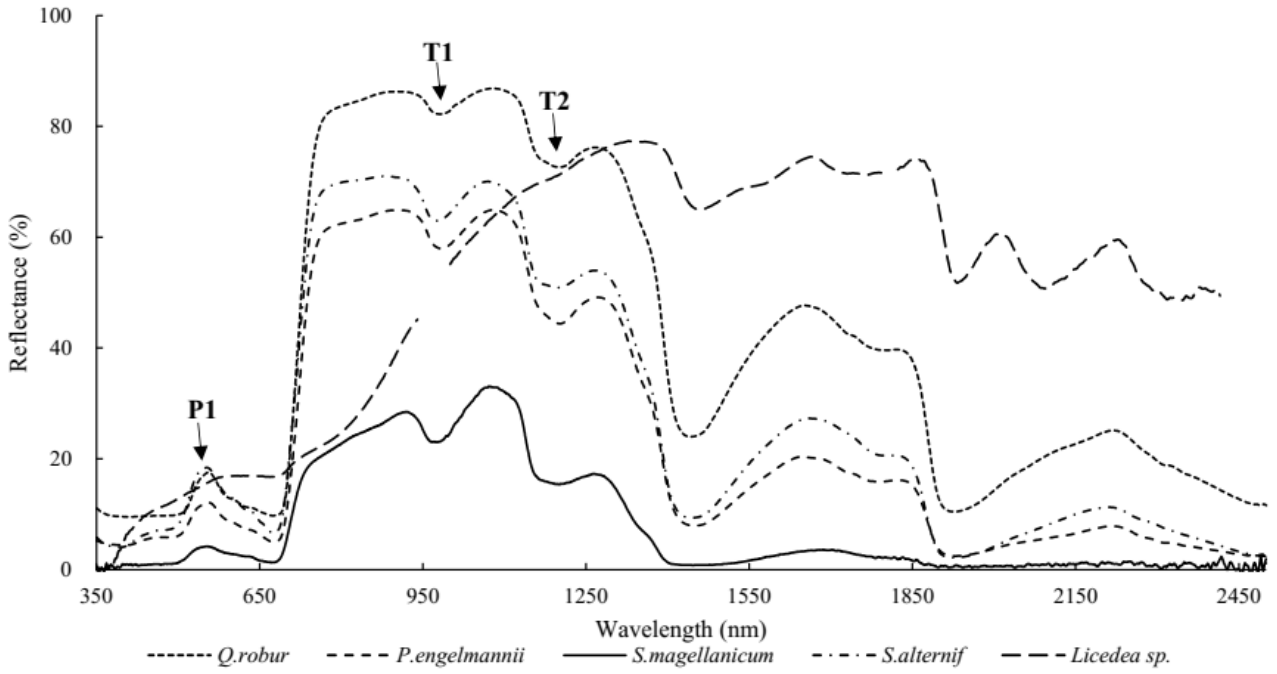

Figure 6. Spectral reflectance of *S. magellanicum* and other plants. P1 indicates a reflectance peak at ~550 nm; T1 and T2 indicate reflectance troughs at ~950 nm and ~1250 nm.

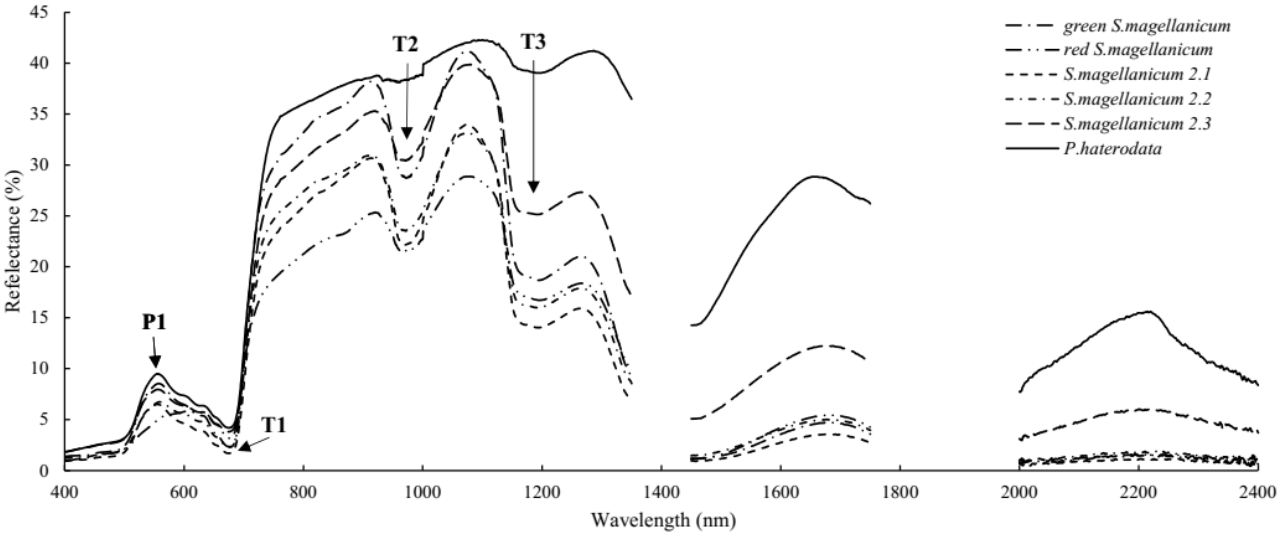

Figure 7. Spectral reflectances of *P. heteroclada* and *S. magellanicum* measured in Plots 1 and 2. P1 indicates a reflectance peak at ~550 nm; T1, T2 and T2 indicate reflectance troughs at ~600 nm, ~980 nm and ~1150 nm. Note that the spectra collected for *S. magellanicum* scenes in Plot 2 are labelled as *S. magellanicum* 2.1, 2.2 and 2.3.

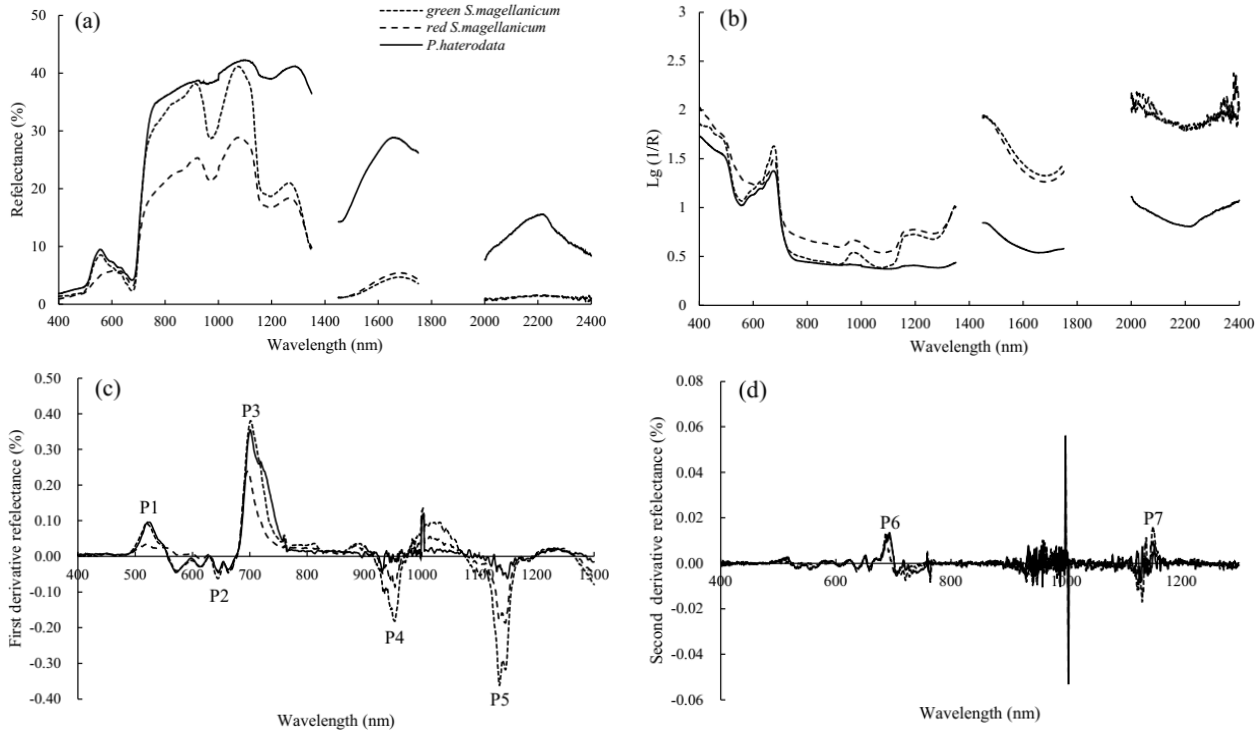

Figure 8. Spectral analysis of *P. heteroclada* Oliver and *S. magellanicum* including: (a) original spectra, (b) lg(1/R) spectra, (c) FDR spectra, and (d) SDR spectra (Pang *et al.* 2019). The labels P1–P7 indicate notable reflectance peaks among plants.

935 nm and 1135 nm (P4 and P5 in Figure 8b). Similarly, the displacement between *P. heteroclada* and *S. magellanicum* of the two peaks at 692 nm and 1150 nm (P6 and P7 in Figure 8d) can be seen on the SDR plot. Overall, the results of spectral analysis (Figures 8b–d) indicate that the crucial spectral range for *S. magellanicum* is around 1150 nm.

Plant attributes and spectral response

Leaf pigment differences

In the VIS, the spectral distinctions between red and green *S. magellanicum* that are controlled by leaf pigment are more pronounced at wavelengths greater than 500 nm. In Figure 9a, the reflectance curves for red and green *S. magellanicum* are low and flat (reflectance range 3–8 %) at 400–500 nm, then rise slowly after 500 nm. For green *S. magellanicum* samples there is a peak (reflectance ~ 4 %) at 550 nm (belonging to yellow-green light), whereas the reflectance of red *S. magellanicum* changes only slightly in the range 500–650 nm without a prominent extreme value. In Figure 9b, the spectra for red and green *S. magellanicum* show a peak shift near 700 nm; that is, the wavelength corresponding to the peak for red *S. magellanicum* (~698 nm) is shorter than that for green *S. magellanicum* (~704 nm). Moreover, red and green *S. magellanicum* have stronger spectral distinctions in the ranges 550–600 and 670–750 nm, indicating that the VIS spectra can be used to identify *Sphagnum* under different growth conditions.

Cell structure

Cross-sections of fresh leaves and a stem are shown in the upper part of Figure 10. *S. magellanicum* has only two distinct cell types. The outer part of the stem is composed of 2–4 layers of polygonal 'hyaline cells' with large transparent lumens, while the internal 'green cells' are nearly circular and contain the photosynthetic pigment chlorophyll. The leaves are monolayers of large and transparent hyaline cells alternating with narrow chlorophyllose ('green') cells. When observing the surfaces of dried leaves under the microscope (lower part of Figure 10), it is clear that the green cells are interwoven into networks interspersed with hyaline cells whose walls are helically thickened and perforated by circular pores (appearing black or transparent in Figure 10), which make *Sphagnum* leaves highly absorbent.

Effects of water content on spectral response

The results of the water content gradient experiment are shown in Figure 11. The more dehydrated *S. magellanicum* becomes, the greater are the green peak values of its spectra in the VIS (400–760 nm). The maximum FDR is in the green, at ~520 nm. The FDR spectra of *S. magellanicum* have good discrimination in the VIS between conditions of water saturation (0 h spectrum) and dehydration (144 h spectrum) (Figure 12).

The NIR (760–1300 nm) spectra rise, and the troughs at 980 nm and 1135 nm disappear, as the water content of the leaves decreases and especially

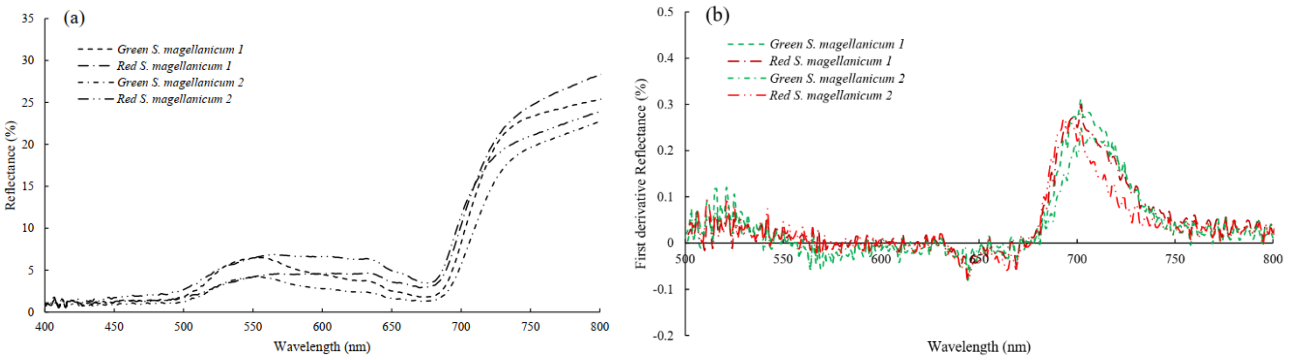

Figure 9. Response of spectra (VIS; 400–760 nm) to pigment changes in *Sphagnum* leaves: (a) the original spectra of the individual scenes of green and red *S. magellanicum* examined in Plot 1, and (b) the corresponding FDR spectra.

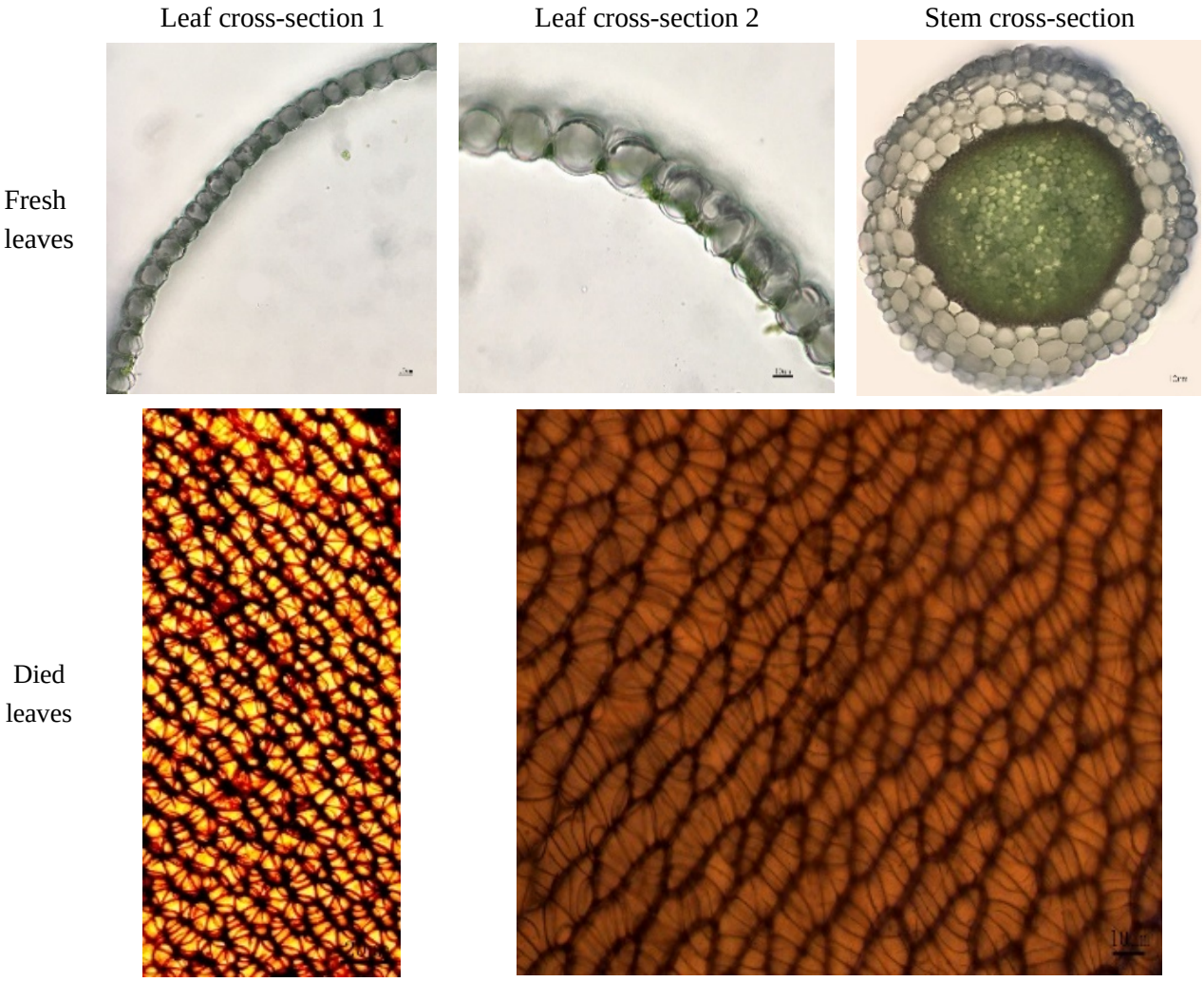

Figure 10. The cell structure of *S. magellanicum* samples.

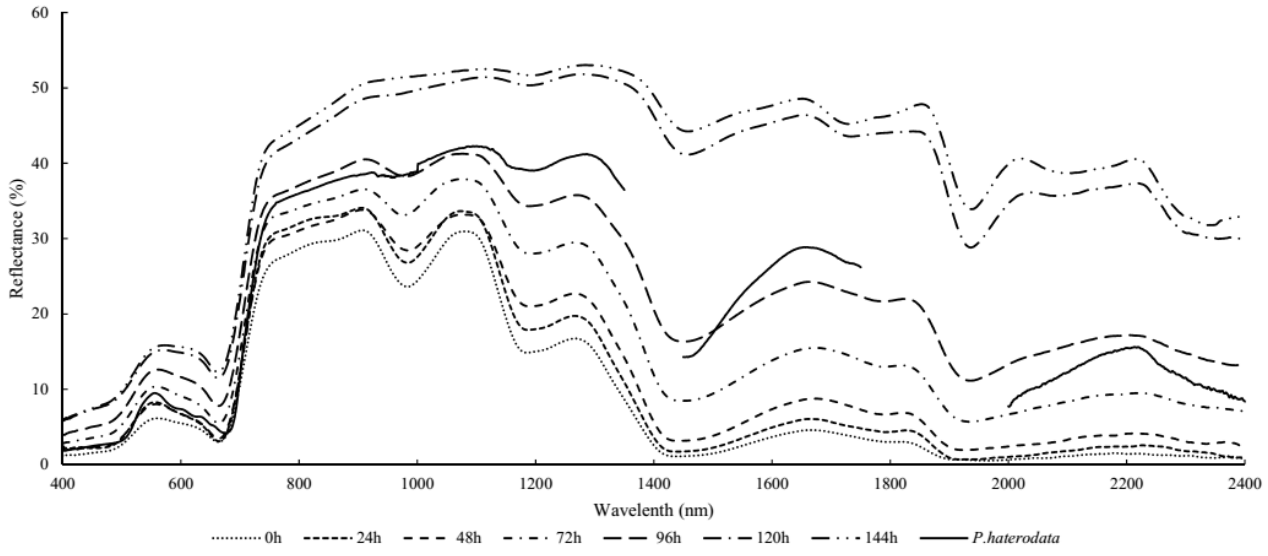

Figure 11. The variation of spectral reflectance with water content in *S. magellanicum*.

when the *S. magellanicum* is completely dehydrated (144 h in Figure 11). The SWIR spectra are particularly sensitive to changes in leaf moisture. When the leaves have lost almost all moisture (120 h and 144 h), the spectra exhibit peaks at 1650, 1850 and 2200 nm and a trough at 1900 nm, which makes them quite different from the spectra under other moisture conditions. Also, the reflectance of *S. magellanicum* is notably higher than that of *P. heteroclada* in the 120 h and 144 h spectra.

Thus, the *S. magellanicum* spectra can be divided into two categories, namely slight water loss (0–96 h) and severe water loss (120 h and 144 h). In the case of slight water loss conditions, the spectra retain properties such as the troughs at 980 and 1135 nm and the peaks at 1650 nm and 2200 nm, which are valuable for distinguishing *Sphagnum* from *P. heteroclada* and other plants. When the moisture is totally lost, the spectral characteristics of *S. magellanicum* change completely, and new spectral rules, based on the spectral reflectance characteristics of peatland vegetation, must be established to distinguish *Sphagnum* from other plants and achieve vegetation mapping.

Spectral characteristics of *S. magellanicum* at the EO sensor level

ASTER has fewer channels in the VIS (400–760 nm) than the other three satellite sensors, meaning that the latter provide better performance for vegetation monitoring. In agreement with the results of laboratory spectral analysis, the sensor equivalent spectral curves of *S. magellanicum* and *P. heteroclada* are less discriminative in the VIS than at longer wavelengths (Figure 13). However, because there are slight differences in the peak at 560 nm between red and green *S. magellanicum*, they are separable using this part of the spectrum. In the NIR (760–1350 nm), the unique spectral properties of *S. magellanicum* begin to stand out. Moreover, the three spectral curves do not coincide in the NIR, especially in ALI and MSI data; thus, these curves illustrate the large disparity between *Sphagnum* and *P. heteroclada*. In the SWIR (1350–2400 nm), the spectral curves of green and red *S. magellanicum* are coincident at first and there are large numerical reflectance gaps relative to *P. heteroclada*. In a vector triangle with 1600 nm as the midpoint and the adjacent bands as the vertices, the spectral angle of

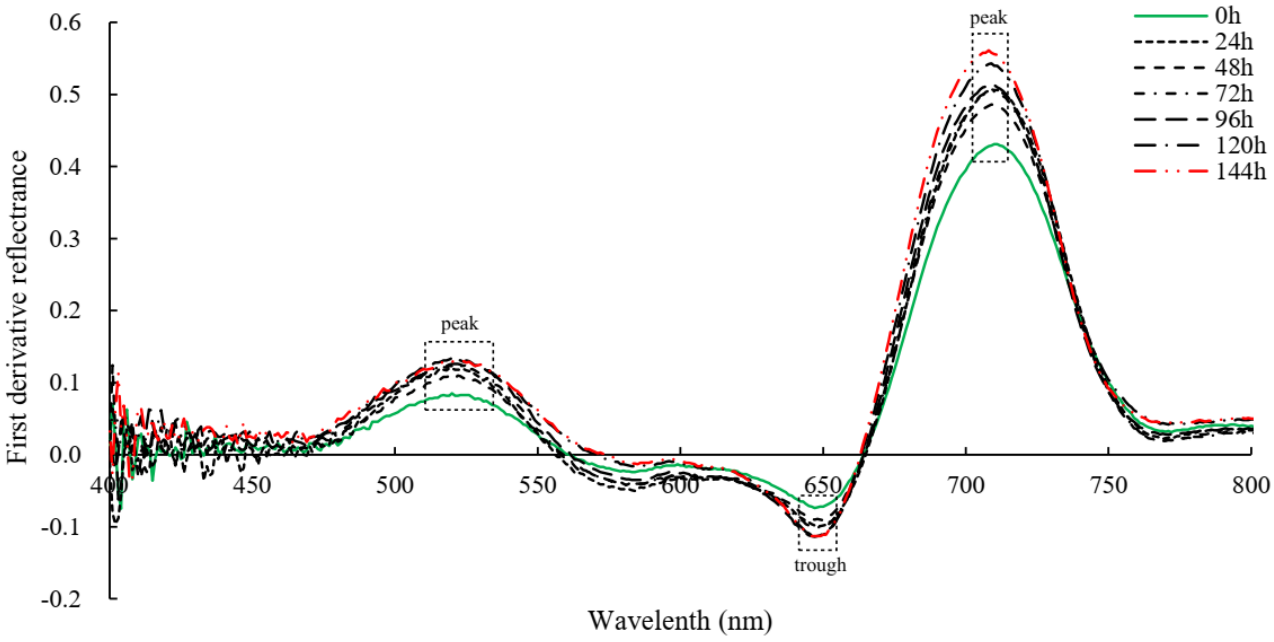

Figure 12. Spectral analysis in VIS under different moisture conditions.

S. magellanicum at 1600 nm is acute (~157°), while that of *P. heteroclada* is obtuse (~183°) (Figure 13c). Therefore, this approach can be used as an effective method to quickly distinguish between *Sphagnum* and other vegetation.

In terms of the vegetation index, the ability of the four sensors to identify *Sphagnum* is relatively consistent. Except for the NDVI, the index values agree quite closely between the different sensors, indicating that there is no wide disparity among sensors used for *Sphagnum* mapping after the correct indicator has been selected. The NDVI and EVI, which are based on the spectral characteristics of vegetation in the VIS-NIR, cannot effectively identify *Sphagnum* but they can be used to distinguish between its different growth conditions (i.e., green or red). In contrast, the MSI (Figure 14c) and NDII (Figure 14c), whose construction is based on the spectral characteristics in the NIR-SWIR, are very good at extracting the *Sphagnum* genus. The NDVI and EVI values of green *S. magellanicum* (0.75 and 0.54, respectively) and *P. heteroclada* (0.70 and 0.52, respectively) are both higher than those of red *S. magellanicum* (0.59 and 0.33, respectively); however, there is a visible value gap between green *S. magellanicum* and *P. heteroclada* in the NDVI only. Therefore, the NDVI and EVI can be used to distinguish red *S. magellanicum* from all of the other species. In the cases of MSI and NDII (Figures 13c, 13d), both *S. magellanicum* and *P. heteroclada* have large numerical gaps. The index value of *P. heteroclada* is much higher than that of *S. magellanicum* for the MSI, and vice versa for the NDII. Thus, it is possible to distinguish effectively between *S. magellanicum* and *P. heteroclada* using the MSI and NDII.

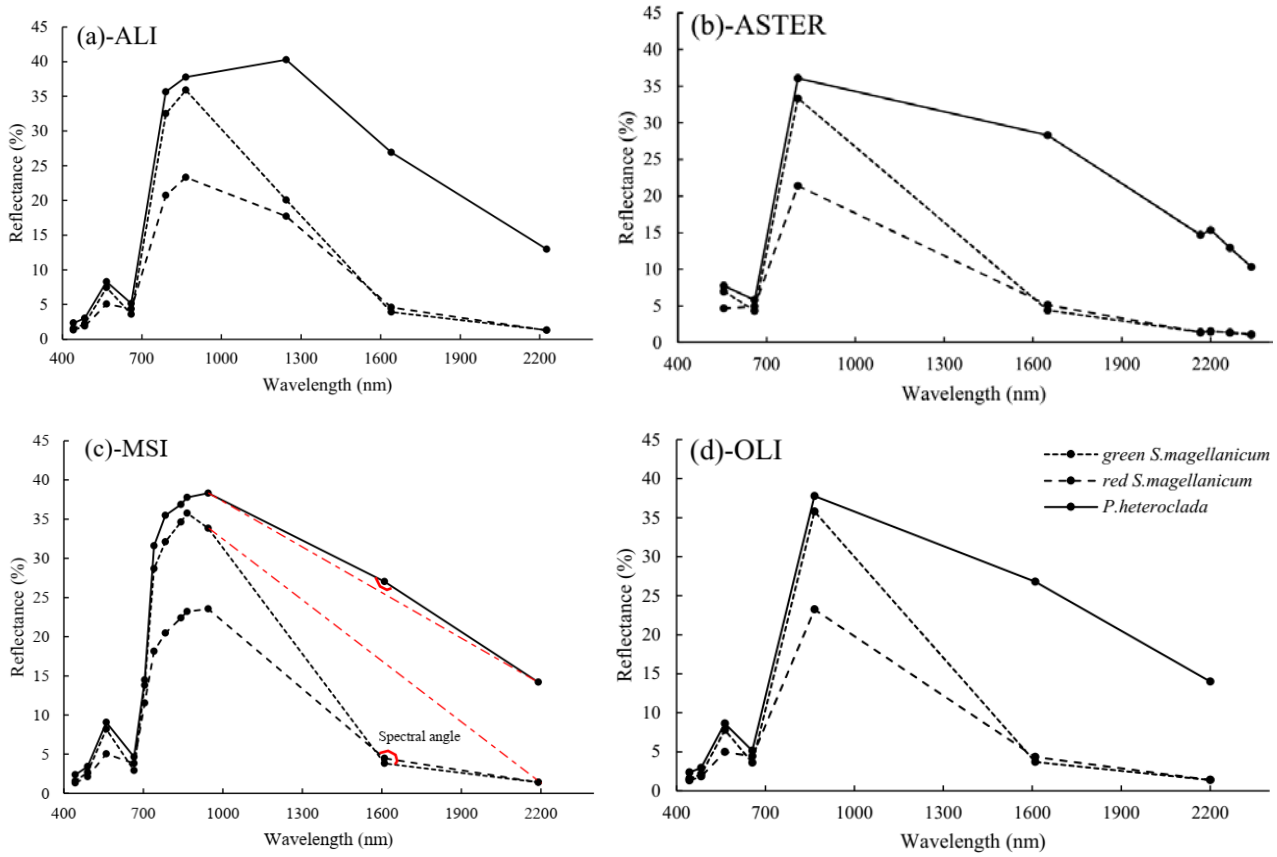

Figure 13. Equivalent sensor spectral curves of *P. heteroclada* and *S. magellanicum*.

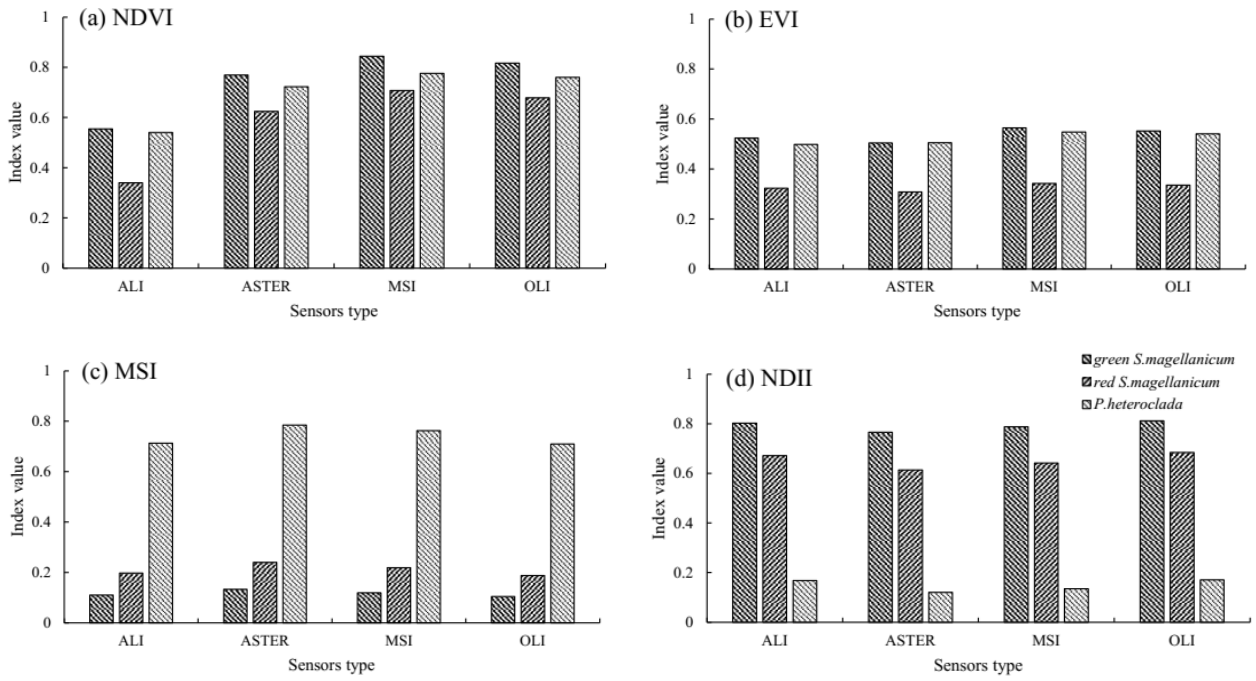

Figure 14. Equivalent spectral indices of *P. heteroclada* and *S. magellanicum* (Pang *et al.* 2019). Note that the EVI values for ASTER were calculated using the formula marked EVI_2 in Table 1, whereas the EVI values for the other three sensors were calculated using the formula marked EVI in Table 1.

DISCUSSION

Spectral characteristics of *Sphagnum*

Comparing the spectral curves of *S. magellanicum* and other plant species (general and specific analyses) showed that *Sphagnum* has its own special spectral characteristics in the NIR-SWIR including, especially, some unique peaks and troughs. In the selected *S. magellanicum* and *P. heteroclada* community, the characteristic bands for the hyperspectral recognition of *S. magellanicum* include the green peak at ~560 nm and the red trough at ~675 nm. In the NIR, the two spectral troughs of *S. magellanicum* at ~980 nm and ~1150 nm visually distinguish it from *P. heteroclada*; and throughout the SWIR, *S. magellanicum* has a much lower reflectance than *P. heteroclada*. Comparison of the VIS spectra of red and green *S. magellanicum* shows that the difference in pigment content changes the wavelength of the peak at ~550 nm, making it feasible also to distinguish between *Sphagnum* of different colours.

Previous studies on *Sphagnum* (Bubier *et al.* 1997, Bryant & Baird 2003) noted that their NIRs were sensitive to water changes and water stress, and this understanding has been gradually applied to hydrological inversion and monitoring of peatland surfaces (Harris 2008, Harris & Bryant 2009). Based on the spectra acquired in this study, the IR can be used as a stable and significant spectral feature to distinguish between *Sphagnum* and other plant species because *Sphagnum* exhibits deep reflectance troughs at 980 nm and 1135 nm. It would be worthwhile to explore whether these features can be used to underpin the identification of species by vegetation experts in the field. Further research should also consider the *Sphagnum* spectra (green and red *S. magellanicum*) in various growth environments, as this information would support accurate mapping of *Sphagnum* habitats at regional scale. Seasonally wet peatlands can be mapped in fine detail by utilising the response of the *Sphagnum* spectrum to changes in pigment and moisture.

Of course, this study has some limitations including the brevity with which it considers the effects of microtopography on vegetation spectra

(Arroyo-Mora *et al.* 2018). In field spectral acquisition, the results will be affected by background noise, which poses challenges in the direct application of these spectra. In fact, there is a scale effect from the local field to the landscape scale. Our study assumes that the spectra of plants collected in the field (scenes ~0.2 m across) are uniform and can represent the landscape scale (the size of a satellite image pixel is 30 × 30 m). In fact, there is a large scaling effect from the scene to the landscape level. Thus, in developing an integrated method for peatland monitoring that combines aerial, space and ground surveys, further attention must be paid to ensuring that small-scale spectral signals are retained on larger pixels.

Physical and physiological analysis of *Sphagnum*

The results of the experiments combining plant physiology and spectra explain the intrinsic reasons for the spectral characteristics of *S. magellanicum* canopies in terms of the singular structure and physiology of this moss. The spectral characteristics that could be used to distinguish *Sphagnum* are mostly related to its extremely simple cell structure and strong water-holding capacity. The simple structure causes the deep troughs at 980 and 1135 nm which distinguish the NIR reflectance spectrum of *Sphagnum* from the spectra of other plants. Additionally, the extremely low reflectance of *Sphagnum* in the SWIR is directly dependent on its strong water-holding capacity. In the severe water loss (122 h and 144 h, Figure 10) stages of the water stress experiment, the *S. magellanicum* IR spectra soared, and the spectra began to resemble the spectra of *P. heteroclada*. These observations suggest that water stress alters the spacing between the cells of *S. magellanicum*, causing the troughs at 980 and 1150 nm to disappear in the 96 h and 144 h spectra. Thus, although the IR spectral characteristics of healthy *Sphagnum* are sufficient to distinguish it from other vegetation, they are greatly altered during periods of water stress - meaning that it is necessary to consider surface hydrology when attempting to distinguish *Sphagnum* from other plants on the basis of spectral information.

The use of moisture spectra for *Sphagnum* species identification and vegetation mapping is a novel and valuable research topic. The previous study by Harris & Bryant (2009) conducted hydrological monitoring of peatlands through groundwater measurement and field spectral collection and established a model relationship between *Sphagnum* spectra and peatland hydrology. Meingast *et al.* (2014) measured two *Sphagnum*-dominant peatland water spectra in field (i.e., small) and large landscapes and established the relationship between spectral index, surface moisture and groundwater level using these surface reflectance data.

Distinguishing *Sphagnum* in satellite remote sensing data

The difference between *P. heteroclada* and *S. magellanicum* is well described in the spectral curves of the four satellite sensors. Sentinel-2A MSI added more channels in both the NIR and the SWIR; therefore, the potential of these sensors for the discrimination of *S. magellanicum* decreases in the following order: MSI>ASTER>OLI>ALI. Recent studies have also shown that Sentinel-2A can monitor the long-term ecology of peatlands and test the response of northern peatlands to various aspects of climate change (Arroyo-Mora *et al.* 2018, Kalacska *et al.* 2018). ALI was able to represent the distinction between *S. magellanicum* and *P. heteroclada* at 1300 nm. Although the results highlight the great potential for remote sensing *Sphagnum* mapping, many problems must still be overcome. For example, *Sphagnum* peatlands are widely developed in boreal areas where cloud and persistent snow cover make the acquisition of high-quality remote sensing data challenging (Asam *et al.* 2018). Moreover, the environmental scale of real peatland vegetation is smaller than the spatial resolution (10 m) of the latest sensor (Sentinel-2A) MSI considered in this study, creating a need to address the scale effect of small *Sphagnum* peatlands with developed micro-morphology (Arroyo-Mora *et al.* 2018). Also, the spectra of *Sphagnum* will be distorted by the aerial parts of vascular plants (Kalacska *et al.* 2015, Harris *et al.* 2015). Although an unmanned aerial vehicle (UAV) has a higher spatial resolution, which helps in obtaining accurate surface information, its high cost is a constraint on wide application in peatland monitoring. Thus, satellite remote sensing is the most important platform for ecological monitoring of peatlands, and practical research that utilises

remotely sensed data must be promoted.

The EVI and NDVI represent green *S. magellanicum* and *P. heteroclada* as a whole, while the IR indices (MSI and NDII) can effectively distinguish between these two species (Figures 14c, 14d). Due to the divergences between green and red *S. magellanicum* in the VIS (400–760 nm), the EVI and NDVI can easily confuse the colour variations of *S. magellanicum* with different types of vegetation or land cover. Using the vegetation indices we tested, a vegetation index constructed using the VIS can be used to detect *Sphagnum* in different seasons, but only if we can obtain the correct distribution of *Sphagnum* in advance. The vegetation indices that can effectively distinguish *Sphagnum* from accompanying vascular plants rely on the IR (900–1200 nm). Therefore, we could construct a more suitable remote sensing method for distinguishing *Sphagnum* based on other NIR-SWIR indices, including use of the vector spectral angle based on the two characteristic troughs at 980 nm and 1135 nm (Figure 12c).

Overall, the results show that the Sentinel-2A MSI performed best on the spectrum for the mixed *S. magellanicum* and *P. heteroclada* community. In terms of the vegetation index, the ability to identify *Sphagnum* based on the NDII and MSI is significantly better than that using the NDVI and EVI. Moreover, there are no significant differences between sensors when relying on these indices to extract *Sphagnum*. Thus, it is crucial to choose the appropriate index for *Sphagnum* remote sensing applications.

ACKNOWLEDGEMENTS

This study was supported by the National Natural Science Foundation of China (no. 41571049), the Zhejiang Provincial Natural Science Foundation (no. LY16D010007) and the Hangzhou Science and Technology Plan Project (no. 20170533B01). We gratefully acknowledge the assistance with setting up field plots in Tianbaoyan National Nature Reserve that was provided by Lipeng Yu from Zhejiang Hynobius Amjiensis National Reserve and Deshou Pan from the Wetland and Wildlife Conservation Centre in Anji County, Zhejiang.

AUTHOR CONTRIBUTIONS

All authors conceived the ideas underlying the study. The experiments were designed primarily by Yuwen Pang and Junfeng Xu. Yuxin Huang collected the spectral data and Yinying Zhou analysed them. Yuhan Wu collaborated on design of the field spectral experiment, identified *Sphagnum* and other plant species in the field, and provided guidance on plant ecology. Finally, the manuscript was written by Yuwen Pang with help from the other authors.

REFERENCES

Arroyo-Mora, J.P., Kalacska, M., Soffer, R., Ifimov, G., Leblanc, G., Schaaf, E.S., Lucanus, O. (2018) Evaluation of phenospectral dynamics with Sentinel-2A using a bottom-up approach in a northern ombrotrophic peatland. *Remote Sensing of Environment*, 216, 544–560.

Asam, S., Callegari, M., Matiu, M., Fiore, G., De Gregorio, L., Jacob, A., Menzel, A., Zebisch, M., Notarnicola, C. (2018) Relationship between spatiotemporal variations of climate, snow cover and plant phenology over the Alps—An earth observation-based analysis. *Remote Sensing*, 10(11), 1757, 26 pp.

Bryant, R.G., Baird, A.J. (2003) The spectral behaviour of *Sphagnum* canopies under varying hydrological conditions. *Geophysical Research Letters*, 30(3), 1134–1138.

Bubier, J.L., Rock, B.N., Crill, P.M. (1997) Spectral reflectance measurements of boreal wetland and forest mosses. *Journal of Geophysical Research*, 102(D24), 29483–29494.

Buermann, W., Saatchi, S., Smith, T.B., Zutta, B.R., Chaves, J.A., Milá, B., Graham, C.H. (2008) Predicting species distributions across the Amazonian and Andean regions using remote sensing data. *Journal of Biogeography*, 35(7), 1160–1176.

Cole, B., Mcmorrow, J., Evans, M. (2014) Spectral monitoring of moorland plant phenology to identify a temporal window for hyperspectral remote sensing of peatland. *ISPRS Journal of Photogrammetry and Remote Sensing*, 90(4), 49–58.

Cord, A.F., Meentemeyer, R.K., Leitao, P.J., Vaclavik, T. (2013) Modelling species distributions with remote sensing data: bridging disciplinary perspectives. *Journal of Biogeography*, 40(12), 2226–2227.

Dahl, T.E., Zoltai, S.C. (1997) Forested northern wetlands of North America. In: Trettin, C.C., Jurgensen, M.F., Grigal, D.F., Gale, M.R. Jeglum, J.K. (eds.) *Northern Forested Wetlands: Ecology and Management*, CRC Press, Boca Raton, 3–17.

Dawson, T.P., Curran, P.J., Plummer, S.E. (1998) LIBERTY—modeling the effects of leaf biochemical concentration on reflectance spectra. *Remote Sensing of Environment*, 65(1), 50–60.

Deering, D.W. (1979). Rangeland reflectance characteristics measured by aircraft and spacecraft sensors. *Dissertation Abstracts International*, B39(7), 3081–3082.

Dise, N.B. (2009) Peatland response to global change. *Scienc*e, 326(5954), 810–811.

Domínguez-Beisiegel, M., Castañeda, C., Mougenot, B., Herrero, J. (2016). Analysis and mapping of the spectral characteristics of fractional green cover in saline wetlands (NE Spain) using field and remote sensing data. *Remote Sensing*, 8(7), 590, 18 pp.

Douma, J.C., Wijk, M.T.V., Lang, S.I., Shaver, G.R. (2007) The contribution of mosses to the carbon and water exchange of arctic ecosystems: quantification and relationships with system properties. *Plant Cell and Environment*, 30(10), 1205–1215.

Gerdol, R. (1996) The seasonal growth pattern of *Sphagnum magellanicum* Brid. in different microhabitats on a mire in the southern Alps (Italy). *Oecologia Montana*, 5(1), 13–20.

Goetz, J.D., Price, J.S. (2015). Role of morphological structure and layering of *Sphagnum* and *Tomenthypnum* mosses on moss productivity and evaporation rates. *Canadian Journal of Soil Science*, 95(2), 109–124.

Gorham, E. (1991) Northern peatlands: role in the carbon cycle and probable responses to climatic warming. *Ecological Applications*, 1(2), 182–195.

Hanson, D.T., Rice, S.K. (2014) *Photosynthesis in Bryophytes and Early Land Plants*. Advances in Photosynthesis & Respiration 37, Springer, Dordrecht, 342 pp.

Hardisky, M.A., Klemas, V., Smart, R.M. (1983). The influence of soil salinity, growth form, and leaf moisture on the spectral radiance of spartina alterniflora canopies. *Photogrammetric Engineering and Remote Sensing*, 49(1), 77–83.

Harris, A. (2008) Spectral reflectance and photosynthetic properties of *Sphagnum* mosses exposed to progressive drought. *Ecohydrology*, 1(1), 35–42.

Harris, A., Bryant, R.G. (2009) A multi-scale remote sensing approach for monitoring northern peatland hydrology: present possibilities and future challenges. *Journal of Environmental Management*, 90(7), 2178–2188.

Harris, A., Bryant, R.G., Baird, A.J. (2005) Detecting near-surface moisture stress in *Sphagnum* spp. *Remote Sensing of Environment*, 97(3), 371–381.

Harris, A., Bryant, R.G., Baird, A.J. (2006) Mapping the effects of water stress on *Sphagnum*: preliminary observations using airborne remote sensing. *Remote Sensing of Environment*, 100(3), 363–378.

Harris, A., Charnock, R., Lucas, R.M. (2015) Hyperspectral remote sensing of peatland floristic gradients. *Remote Sensing of Environment*, 162, 99–111.

Huang, C.Y. (2009) The *Sphagnum* bog plant resources in Tianbaoyan Nature Reserve in Fujian. *Journal of Fujian Forestry Science and Technology*, 36(1), 134–138.

Hunt, E.R.Jr., Rock, B.N. (1989) Detection of changes in leaf water content using Near- and Middle-Infrared reflectances. *Remote Sensing of Environment*, 30(1), 43–54.

Jacquemoud, S., Baret, F. (1990) PROSPECT: a model of leaf optical properties spectra. *Remote Sensing of Environment*, 34(2), 75–91.

Jiang, Z., Huete, A.R., Didan, K., Miura, T. (2008). Development of a two-band enhanced vegetation index without a blue band. *Remote Sensing of Environment*, 112(10), 3833–3845.

Kalacska, M., Lalonde, M., Moore, T.R. (2015) Estimation of foliar chlorophyll and nitrogen content in an ombrotrophic bog from hyperspectral data: scaling from leaf to image. *Remote Sensing of Environment*, 169, 270–279.

Kalacska, M., Arroyo-Mora, J.P., Soffer, R.J., Roulet, N.T., Moore, T.R., Humphreys, E., Leblanc, G.,

Lucanus, O., Inamdar, D. (2018) Estimating peatland water table depth and net ecosystem exchange: A comparison between satellite and airborne imagery. *Remote Sensing*, 10(5), 687, 25 pp.

Kokaly, R.F., Clark, R.N., Swayze, G.A., Livo, K.E., Hoefen, T.M., Pearson, N.C., Wise, R.A., Benzel, W.M., Lowers, H.A., Driscoll, R.L., Klein, A.J. (2017) *USGS Spectral Library Version 7*. Report Data Series 1035, US Geological Survey, Reston VA, 61 pp. Online at: https://pubs.er.usgs.gov/publication/ds1035, accessed 20 Jly 2020.

Kremer, C., Pettolino, F., Bacic, A., Drinnan, A. (2004) Distribution of cell wall components in *Sphagnum* hyaline cells and in liverwort and hornwort elaters. *Planta*, 219(6), 1023–1035.

Kyrkjeeide, M.O., Hassel, K., Flatberg, K.I., Shaw, A.J., Yousefi, N., Stenøien, H.K. (2016) Spatial genetic structure of the abundant and widespread peatmoss *Sphagnum magellanicum* Brid. *PLoS ONE*, 1111(2), e0148447, 19 pp.

Letendre, J., Poulin, M., Rochefort, L. (2008) Sensitivity of spectral indices to CO_2 fluxes for several plant communities in a *Sphagnum*-dominated peatland. *Canadian Journal of Remote Sensing*, 34(sup2), S414–S425.

Limpens, J., Berendse, F., Blodau, C., Canadell, J. G., Freeman, C., Holden, J., Roulet, N., Rydin, H., Schaepman-Strub, G. (2008) Peatlands and the carbon cycle: from local processes to global implications - a synthesis. *Biogeosciences*, 5(6), 1475–1491.

Liu, K., Zhao, D., Fang, J., Zhang, X., Zhang, Q., Li, X. (2017) Estimation of heavy-metal contamination in soil using remote sensing spectroscopy and a statistical approach. *Journal of The Indian Society of Remote Sensing*, 45(5), 805–813.

Mendes, C., Dias, E. (2013) Classification of *Sphagnum* peatlands in Azores — cases from Terceira Island. *Suo*, 64(4), 147–163.

Meingast, K.M., Falkowski, M.J., Kane, E.S., Potvin, L.R., Benscoter, B.W., Smith, A.M.S., Borgeau-Chavez, L.L., Miller, M.E. (2014) Spectral detection of near-surface moisture content and water-table position in northern peatland ecosystems. *Remote Sensing of Environment*, 152, 536–546.

Pang, Y.W., Huang, Y.X., Wen, J.Y., Xu, J.F. (2019) Study on the spectral characteristics and remote sensing recognition of the *Sphagnum* community. *Plant Science Journal*, 37(2), 125–135.

Plaza, A., Benediktsson, J.A., Boardman, J.W., Brazile, J., Bruzzone, L., Camps-Valls, G., Chanussot, J., Fauvel, M., Gamba, P., Gualtieri, A., Marconcini, M., Tilton, J.C., Trianni, G. (2009) Recent advances in techniques for hyperspectral image processing. *Remote Sensing of Environment*, 113(supp-S1), S110–S122.

Pu, R., Yu, Q., Gong, P., Biging, G.S. (2005) EO-1 Hyperion, ALI and Landsat 7 ETM+ data comparison for estimating forest crown closure and leaf area index. *International Journal of Remote Sensing*, 26(3), 457–474.

Radoux, J., Chomé, G., Jacques, C.D., Waldner, F., Bellemans, N., Matton, N., Lamarche, C., d'Andrimont, R., Defourny, P. (2016) Sentinel-2's potential for sub-pixel landscape feature detection. *Remote Sensing*, 8(6), 488, 28 pp.

Richardson, A.D., Hufkens, K., Milliman, T.E., Aubrecht, D.M., Furze, M.E., Seyednasrollah, B., Krassovski, M.B., Latimer, J.M., Nettles, W.R., Heiderman, R.R., Warren, J.M., Hanson, P.J. (2018) Ecosystem warming extends vegetation activity but heightens vulnerability to cold temperatures. *Nature*, 560(7718), 368–371.

Rydin, H., Jeglum, J.K. (2006) *The Biology of Peatlands*. Oxford University Press, 354 pp.

Schubert, P., Eklundh, L., Lund, M., Nilsson, M. (2010) Estimating northern peatland CO_2 exchange from MODIS time series data. *Remote Sensing of Environment*, 114(6), 1178–1189.

Schultheis, E.H., Hopfensperger, K.N., Brenner, J.C. (2010) Potential impacts of climate change on *Sphagnum* bogs of the southern Appalachian Mountains. *Natural Areas Journal*, 30(4), 417–424.

Sonnentag, O., Chen, J.M., Roberts, D.A., Talbot, J., Halligan, K.Q., Govind, A. (2007) Mapping tree and shrub leaf area indices in an ombrotrophic peatland through multiple endmember spectral unmixing. *Remote Sensing of Environment*, 109(3), 342–360.

Tutschek, R. (1982) Interference of l-α-aminooxy-β-phenylpropionic acid with cold-induced sphagnorubin synthesis in *Sphagnum magellanicum* BRID. *Planta*, 155(4), 307–309.

Van Gaalen, K.E., Flanagan, L.B., Peddle, D.R. (2007) Photosynthesis, chlorophyll fluorescence and spectral reflectance in *Sphagnum* moss at varying water contents. *Oecologia*, 153(1), 19–28.

Vitt, D.H., Wieder, R.K. (2008) The structure and function of bryophyte-dominated peatlands. In: Goffinet, B., Shaw, A.J. (eds.) *Bryophyte Biology*, Cambridge University Press, 357–392.

Vogelmann, J.E., Moss, D.M. (1993) Spectral reflectance measurements in the genus *Sphagnum*. *Remote Sensing of Environment*, 45(3), 273–279.

Wang J.D., Zhang, L.X., Liu, Q.H. (2009) *Spectral Knowledge Base of Typical Ground Objects in China*. Science Press, Beijing, 1.

Wardlow, B.D., Egbert, S.L., Kastens, J.H. (2007). Analysis of time-series MODIS 250 m vegetation index data for crop classification in the US Central Great Plains. *Remote Sensing of Environment*, 108(3), 290–310.

Whinam J, Copson G. (2006) *Sphagnum* moss: an indicator of climate change in the sub-Antarctic. *Polar Record*, 42(1), 43–49.

Wu, J. (2012) Response of peatland development and carbon cycling to climate change: a dynamic system modeling approach. *Environmental Earth Sciences*, 65(1), 141–151.

Wu, J., Peng, D. (2011) Advances in researches on hyperspectral remote sensing forestry information-extracting technology. *Spectroscopy and Spectral Analysis*, 31(9), 2305, 12 pp.

Xiao, S., Zhang, Z., You, W., Liu, J., Wu, J. (2018) Soil microbial community composition in four *Nothotsuga longibracteata* forests in southern China. *Polish Journal of Environmental Studies*, 27(2), 917–925.

Xie, Y., Sha, Z., Yu, M. (2008) Remote sensing imagery in vegetation mapping: a review. *Journal of Plant Ecology*, 1(1), 9–23.

Yu, Z.C. (2012) Northern peatland carbon stocks and dynamics: a review. *Biogeosciences*, 9(10), 4071–4085.

Submitted 20 Jly 2019, final revision 22 Jly 2020
Editor: Olivia Bragg

Author for correspondence: Junfeng Xu, Institute of Remote Sensing and Geoscience, Hangzhou Normal University, Zhejiang, China. E-mail: junfeng_xu@163.com